

Bulletin of Materials Science & Metallurgy

Periodical Scientific Journal of UCTEA Chamber of Metallurgical and Materials Engineers

Received: 11 April 2025

Volume 2, Issue 2, 2025, Pages 6-13 https://doi.org/10.70342/EFHM8547

Accepted: 08 October 2025

Research Article

Investigation of Sintering Temperature Effect on Scandate Cathode Pore Structure and Mathematical Expression

Zeynep Hazal Yazğan^{a,*} , Nergis Yıldız Angın Atmaca^b and Okan Mert Yücedağ^c

^aDepartment of Metallurgical and Materials Engineering, Istanbul Technical University, Istanbul, Türkiye ^bTÜBİTAK BİLGEM, Kocaeli, Türkiye

^cRST Technology, Türkiye

*Corresponding author's email: yazgan25@itu.edu.tr

Abstract

In this study, changes in the surface pore structure depending on the sintering temperature of the cathodes used in vacuum electronic devices were investigated. Ammonium meta tungstate (AMT) $[(NH_4)_6(H_2W_{12}O_4O)_4H_2O](99.9\%$ w/w), Sc(NO₃)₃(99.99% w/w), and 4:1:1 barium calcium aluminate (BCA) were purchased and used without further purification. Tungsten powders were doped with scandium nitrate and BCA. After synthesizing the powder, consecutive material characterization analyses were conducted. The sintering processes were carried out at different temperatures in a hydrogen atmosphere and the pore structure was studied in detail by SEM and EDS analyses.

The experimental data were analysed with a mathematical modelling to investigate the relationship between sintering temperature and pore diameters. Two pieces of function were utilized to describe the pore size and sintering temperature relation. The effect of sintering temperature on the pore structures of the cathode surface has been studied and the importance of pore dimensions on cathode performance and life has been emphasized. Therefore, this mathematical modelling offers a promising prediction technique by saving time and cost.

Keywords

scandate cathode, sintering, pore structure, mathematical modelling

1. Introduction

In vacuum electronic devices, cathodes are used as an electron source which is required for electron beam energy supply to the system [1]. So, there are some basic needs for dispenser cathodes such as high current density and long lifetime [2]. To meet these needs, scandate thermionic cathodes have been attracting great attention for decades [3]. They exhibit most up-to-date properties among the other dispenser cathode species in terms of higher current density, lower operating temperature and longer life [4]. However, when the current density of the cathodes is higher, the emission performance of the cathode deteriorates due to the gases released. Therefore, it is crucial for a cathode to have ion bombardment resistant pore structures [5]. Thus, the surface characteristics of scandate pellets should be analysed in detail.

Tungsten is generally used as a fundamental matrix material for cathodes and powder metallurgical techniques are used for fabrication of cathodes in most cases [6]. Powder particle shape, dimension, purity, sintering parameters and pore

characteristics of the sintered pellet directly affect the performance of cathodes. In this study, all of the scandate cathode fabrication materials were prepared in spray dryer device so as to collect homogeneous powders. In literature, there are various kind of scandate cathode production types. The main focus is based on fabrication of these types of cathodes such as traditional impregnated scandate cathodes, top layer cathodes, impregnated mix matrix scandate cathodes, pressed scandate cathodes and spray dried scandate cathodes [7]. The majority of works in this field is experimental. There is a lack of studies in the literature that incorporate computational inductive methodologies based on experimental data. This is exactly the point at which the novel aspect of our study becomes significant. In this study, both the most advanced manufacturing technology was employed and a model was developed to establish the relationship between sintering temperature and cathode pore size based on experimental data. To the best of our knowledge, there is no study in the literature that uses experimental sintering temperature data to investigate the relationship with pore size.

Characterization studies including X-Ray Diffractometer (XRD), Scanning Electron Microscope (SEM), Energy Dispersive Spectrometer (EDS) were performed. After getting proper chemical forms and amounts, cold isostatic pressing and sintering studies were conducted. The pellets were sintered at different temperatures to observe the temperature effects on the pore structures. Surface porosity, shrinkage values and pore sizes were analysed and calculated. Pore size values were correlated with sintering temperatures. Finally, it was obtained a mathematical relation that explains the sintering behaviour of pellets and pore size alteration with temperature. Thus, one can easily estimate the pore sizes before sintering procedure in advance.

2. Materials and Methods

2.1. Preparation of co-doped tungsten (CDT) powder

Commercial AMT [(NH₄)₆(H₂W₁₂O₄₀)₄H₂O] (99.9% w/w), scandium nitrate (Sc(NO₃)₃) (99.99% w/w), and 4:1:1 BCA were used as raw materials. CDT powders were prepared by dissolving AMT, Sc(NO₃)₃, and BCA in water followed by spray drying method with combined calcination and hydrogen reduction processes. The solution which is composed of AMT, Sc(NO₃)₃ and BCA was mixed and a homogeneous powder was obtained. In order to ensure the homogeneity and sphericality of the powder, many experiments were conducted. In the final stage, it can be seen in Figure 1 that we have achieved the desired form.

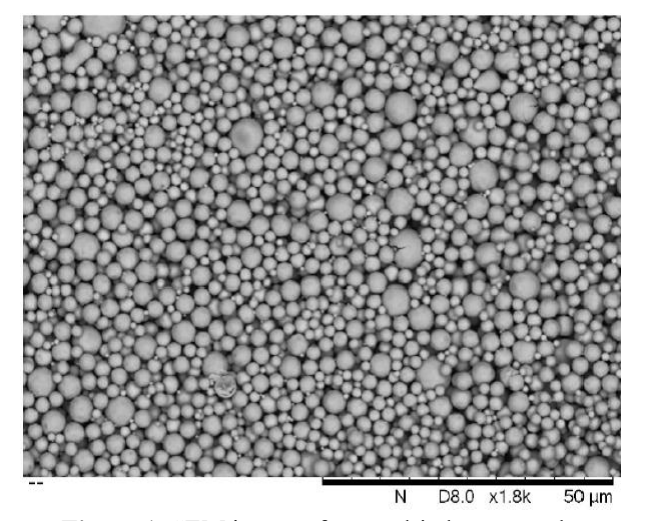


Figure 1. SEM image of spray dried raw powder

In Figure 2, the powder production steps are explained and given below:

- 1: Scandium nitrate, AMT and BCA water solution which is used in spray drying
- 2: Raw powder SEM analysis after spray drying
- 3: Raw powder physical form is calcinated in ceramic furnace
- 4: Calcinated powder is reduced in hydrogen atmosphere

This procedure is performed sequentially in an iterative manner until getting the aimed homogeneous powder form.

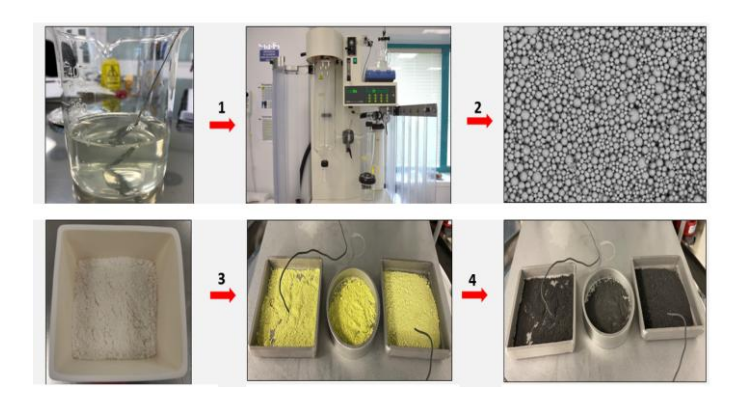


Figure 2. Cathode powder fabricating process steps

2.2. Microstructure characterization and analyses

raw obtaining mixed powder, consecutive characterization methods were applied in order to identify the properties of powder. Raw powders were subjected to heat treatment to reduce them. Phase identification of reduced CDT (r-CDT) powder was investigated with an XRD, which was carried out using Cu Ka radiation at 40 kV and 20 Ma. The particle size was analysed with a Malvern Instruments MASTERSIZER 2000. SEM-EDS was used to characterize morphology of powders and sintered r-CDT pellet. Pore size measurements of r-CDT pellets were completed, and average pore sizes were calculated from SEM image data sets for each sintering condition by using ImageJ software. Porosity can be calculated as a ratio of the area of pores to the total area of sample analysed [8]. Therefore, SEM images were collected to calculate the porosity % of r-CDT sintered at different temperatures (Equation 1):

$$P\% = \frac{Pores\ Area}{Total\ Area} x 100 \tag{1}$$

Conducted experiment data were analysed and modelling studies were conducted.

The powder was spray dried first, then calcined in air atmosphere and finally reduced one more time in hydrogen atmosphere.

At the final stage, scandia doped tungsten powder was obtained. The pellet structures were fabricated with cold isostatically pressing technique. They were prepared for sintering process.

2.3. Sintering Process

r-CDT powders were cold isostatically pressed and then sintered at 1425, 1500, 1575, 1650, 1725, 1800 °C in the controlled atmosphere. Tungsten is generally sintered at high temperature above 2000 °C to gain full density. However, there is no need of full density for some cathode applications. Therefore, sintering temperature of tungsten can be reduced to control of the microstructure by alternative techniques [9]. It

is explained in literature that, sintering temperature of tungsten is between 1500-2200 °C to form porous matrix for cathode application [10]. In present study, lower sintering temperature is chosen as 1425 °C because barium-containing compound (BaWO₄ and Ba₂CaWO₆) which formed after reduction, melts temperature above 1400 °C [11].

In this study, upper limit is chosen as 1800 °C because extrahigh sintering temperature is not preferred to prevent it from melting away. In previous studies, sintering temperature for barium tungsten cathode is preferred 1800-1900 °C [12].

3. Experimental Results and Discussion

Particle size distribution of doped tungsten powder is given in Figure 3. The powder particle size was measured as approximately $7\,\mu m$.

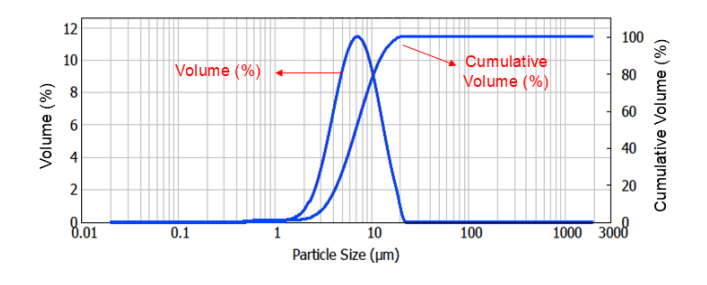
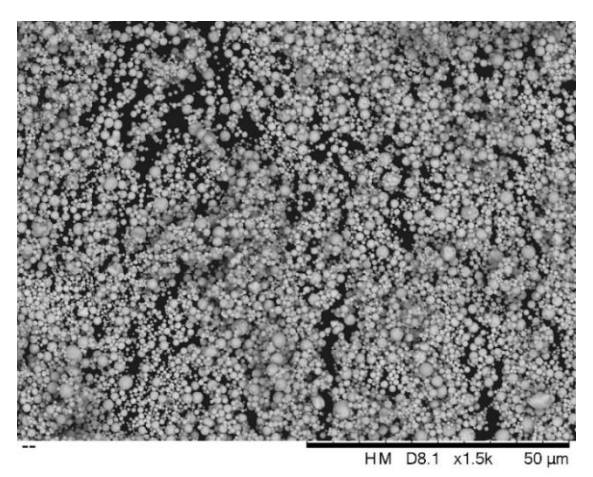
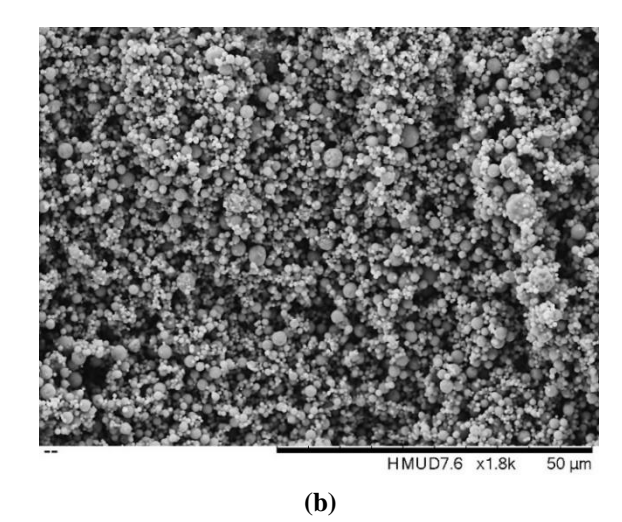


Figure 3. Particle size distribution of doped tungsten powder

The SEM images of processed powder are shown in Figure 4. As it can be seen, the particles maintain their spherical shape. The SEM images show that with the increasing effect of heat treatment on samples, the particle size of samples was progressively decreased.



(a)



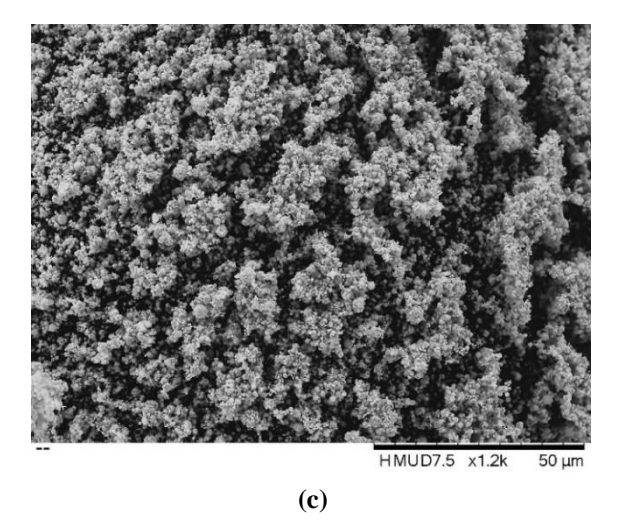
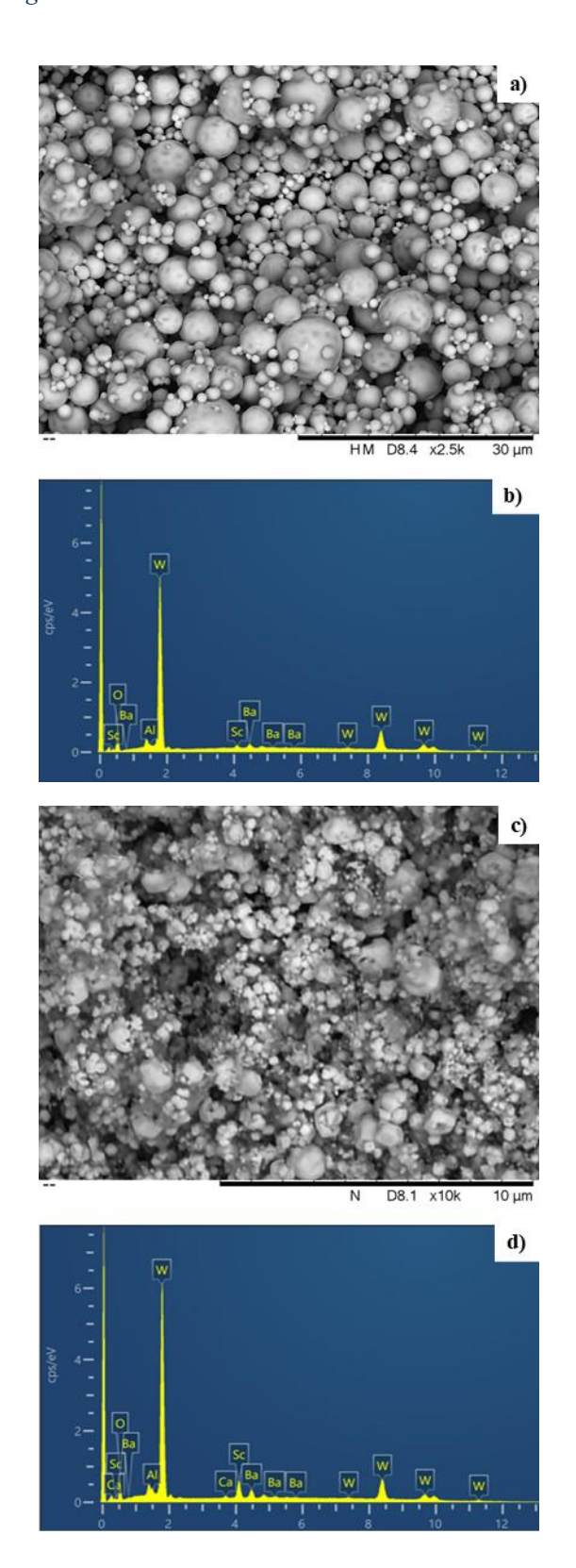


Figure 4. SEM image of (a) raw powder form after spray drying (b) raw powder after calcination (c) powder after hydrogen reduction

The SEM-EDS analyses of the CDT and r-CDT are given in Figure 5. As shown Figure 5 (a) CDT powder prepared by spray drying have spherical shape without agglomeration. After reduction, r-CDT retained its spherical shape but with agglomeration. It can be seen that particle size of r-CDT is smaller than calcined CDT. On the other hand, it's reported that fine grains form due to pinning effect after reduction [13]. The average size of r-CDT powder particles has been measured to be approximately 6-7 μ m, indicating that the material predominantly consists of fine grains. Due to their small size, these fine grains tend to aggregate, as seen in the Figure 5 (c-e). When Figure 5 (e-f) is investigated, scandia is distributed homogenously in both areas. In literature, it is explained that uniform distribution of scandia increases the emission performance of cathodes [13].



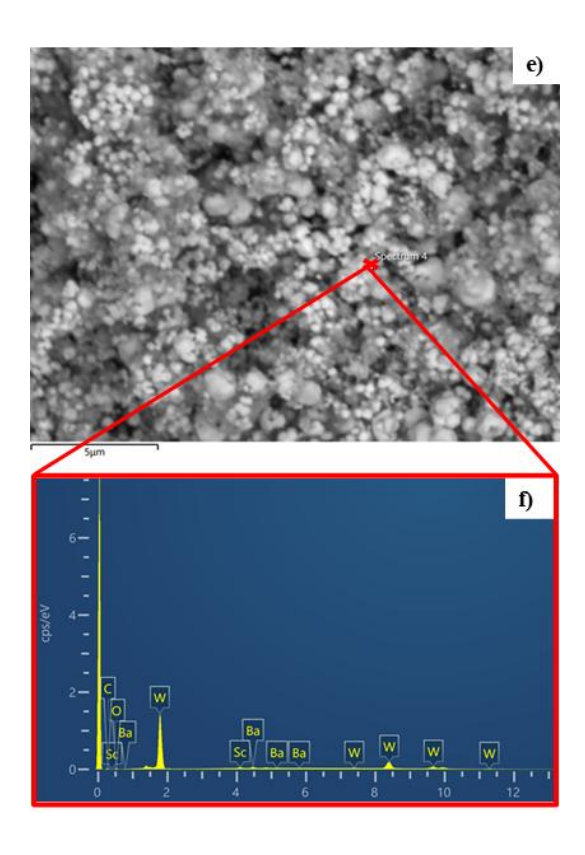


Figure 5. a) SEM and b) EDX of CDT powder, c-e) SEM and d-f) EDX of r-CDT powder

Figure 6 shows XRD pattern of r-CDT. It has been determined that the r-CDT mainly consists of W, Sc_2O_3 , $BaWO_4$ and Ba_2CaWO_6 phases (Figure 6). Ba_2CaWO_6 is known as ternary compound in CaO-BaO-WO₃ system. Also, Ba_2CaWO_6 phase reacts with W and transforms into $3(Ba_{1/3}Ca_{2/3})WO_4$ and Ba (Equation 2) [11].

$$2Ba_2CaWO_6 + W \rightarrow 3(Ba_{1/3}Ca_{2/3})WO_4 + Ba$$
 (2)

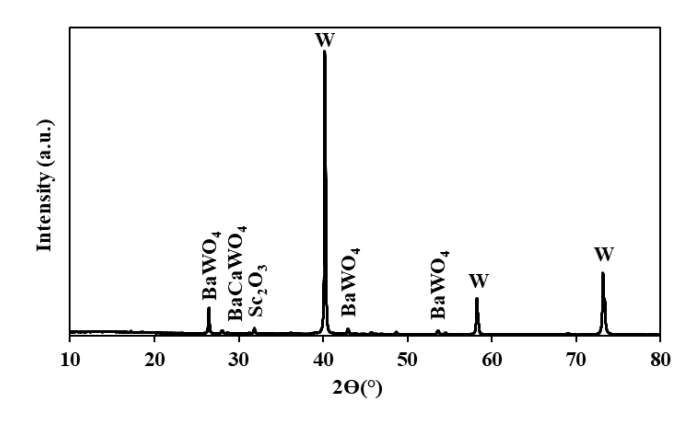
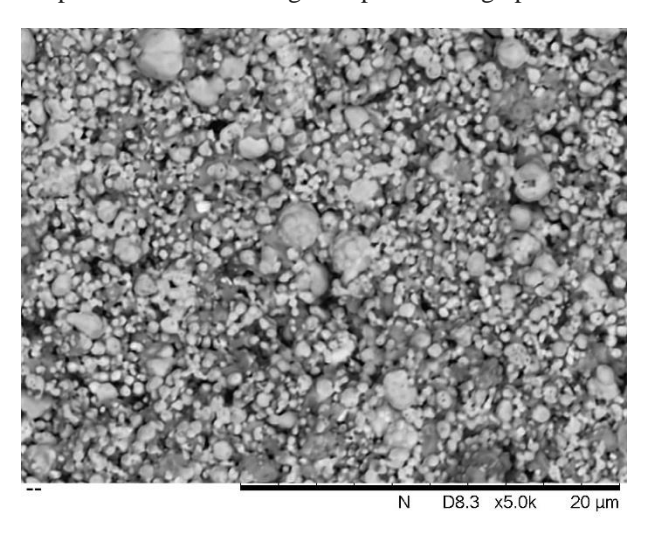


Figure 6. XRD pattern of r-CDT powder

Figure 7 represents that the differences between pellet surfaces. It is apparent that the pores of the pellet structure are interconnected, and sintering has occurred. In addition to

sintering, impregnant materials are observed apparently on the surface. Some pores are full of impregnates and some of them are empty. This is a proper structure that can allow free barium to evaporate and flow through the pores during operation.



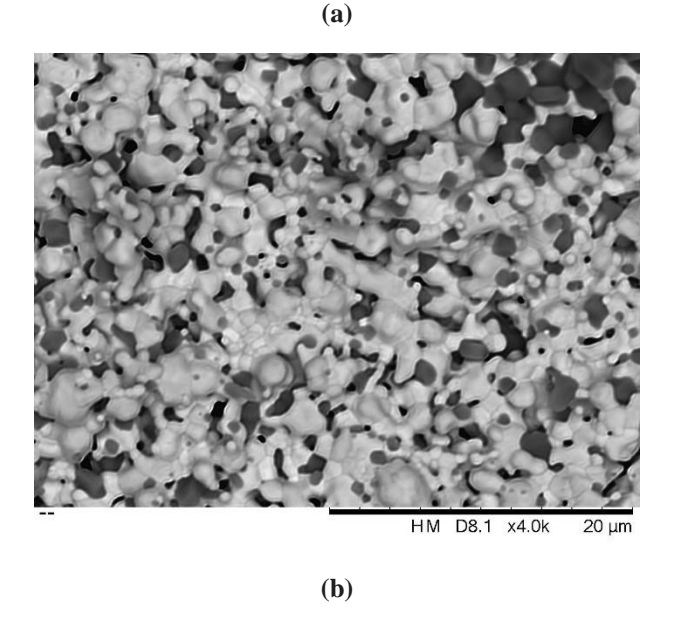


Figure 7. SEM images of pellets after sintering at (a) 1425 °C and (b)1800 °C

Relationship between volume shrinkage and sintering temperature is shown in Figure 8 (a). As the temperature increases, volume shrinkage increased from 4% to 28%. This situation indicates that sintering continues with increasing temperature, and that further temperature increments can contribute to densification. Average pore sizes at different temperature are presented in Figure 8 (b). From 1425 °C to 1650 °C, average pore size increased with increasing temperature, while, above 1650 °C, average pore size decreased. Calculated total porosity according to Equation 1 is shown in Figure 8 (c). As the sintered temperature increases from 1425 °C to 1500 °C, porosity remained the same and

increased until 1650 °C. However, after 1650 °C, it decreased steeply from 11% to 4%. As can be seen on Figure 8 (c) porosity changes as a function of sintering temperature [14]. Pore size distribution shifted towards the higher radius side as increasing temperature from 1425 °C to 1650 °C. At 1725 °C, the pores within 1.2-1.4 μm could not be detected. Therefore, pore size distribution curves shifted towards the left.

Based on the results, sintering process can be classified in three stages according to pore size variation with temperature as shown in Figure 8 (b). So, the first stage is called initial phase in which pore growth is insignificant with temperature change. The second stage is called intermediate phase that pore size increase dramatically until the temperature reaches the sintering value. It is known that pore growth in intermediate stage can be related to particle arrangement occurring by diffusion [15]. As expected, the larger sized pores relative to the initial phase are observed in pore size distribution in Figure 9. However, because of the pores are united with the grain boundaries and eliminated with diffusion in the final stage, a decrease in the pore size may occur [16].

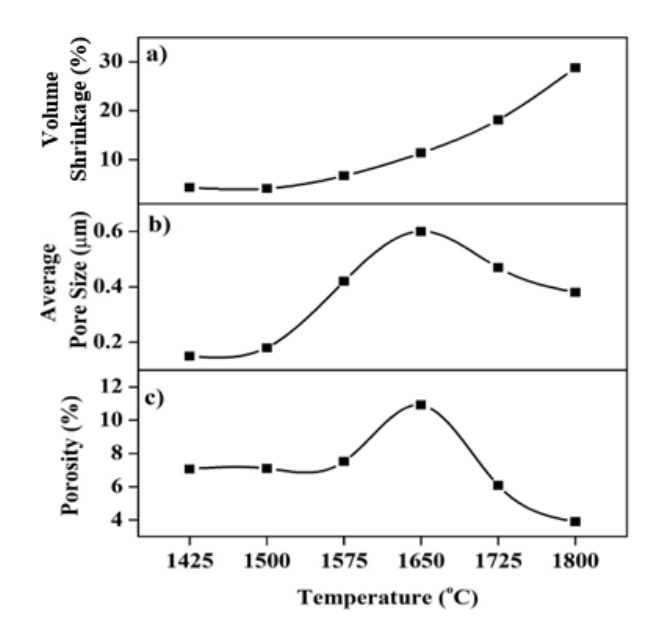


Figure 8. a) Volume shrinkage, b) average pore size and c) porosity of sintered r-CDT at different sintering temperature

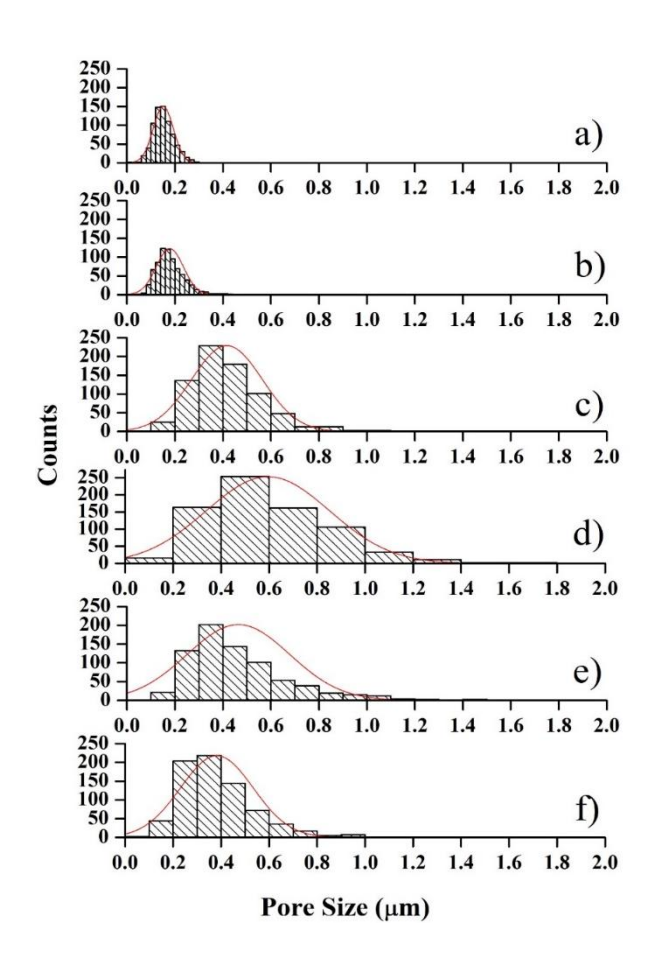


Figure 9. Pore size distribution of sintered r-CDT at different sintering temperature (a. 1425 °C, b. 1500 °C, c. 1575 °C, d. 1650 °C, e. 1725 °C, f. 1800 °C)

SEM and processed (by thresholding) images of the r-CDT sintered different temperatures are shown in Figure 10. When it is examined processed (by thresholding) images of the r-CDT sintered, it is observed that pores are interconnected at 1425 °C and 1500 °C (Figure 10 (b) and Figure 10 (d)). With increasing temperature pores are closed (isolated). Above 1650 °C, pores break into smaller pores. As can be seen on the Figure 8 (b), pore size decreases above 1650 °C. Therefore, processed images are consistent with Figure 8 (b).

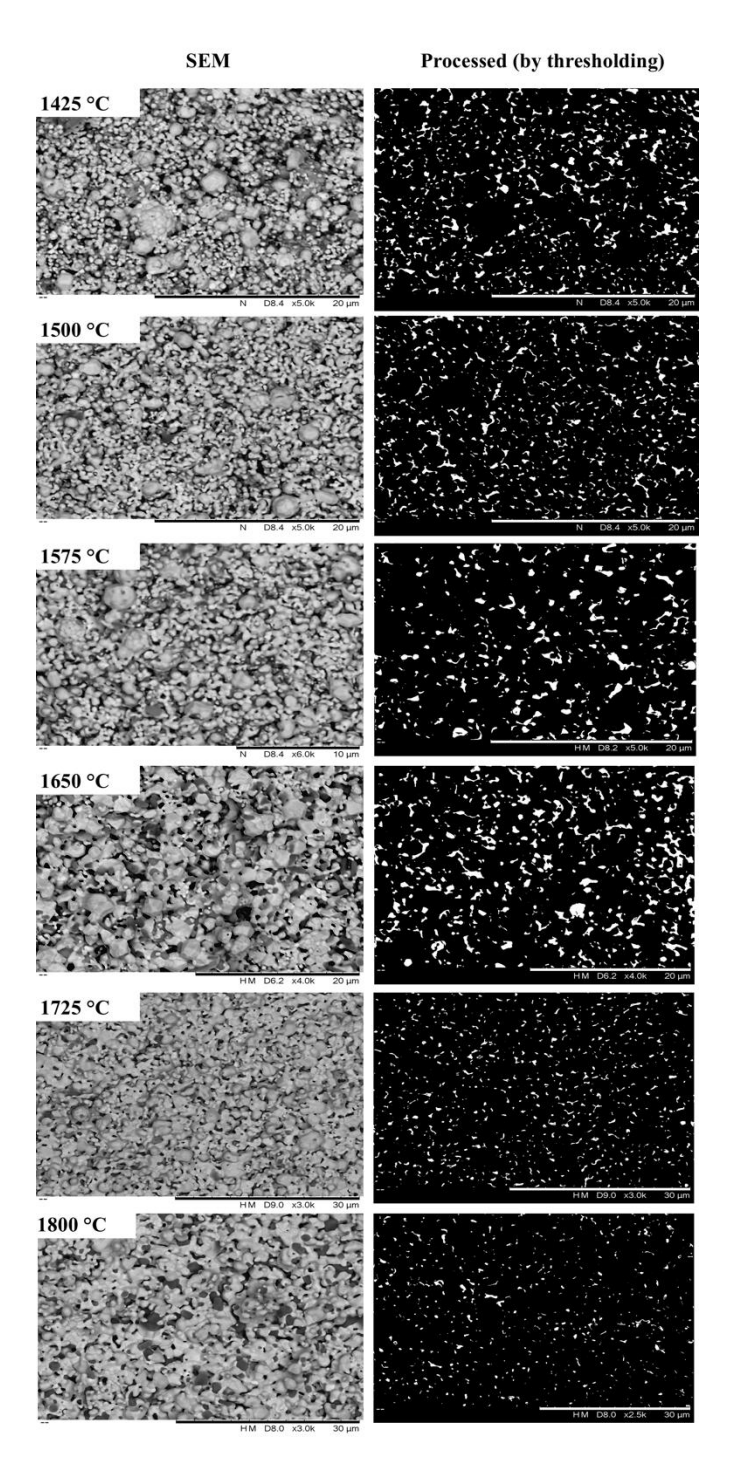


Figure 10. SEM and processed (by thresholding) images of the r-CDT sintered at different temperatures

The data collected from pellets are gathered and summarized in Table 1 as below.

Table 1. Pellet surface data after sintering

Sintering temperature (°C)	Pore size (µm)	Volume shrinkage (%)	Surface porosity (%)
1425	0.15	4.27	7.06
1500	0.18	4.1	7.1
1575	0.42	6.7	7.52
1650	0.6	11.34	10.91
1725	0.47	18.1	6.08
1800	0.38	28.77	3.9

The avereage pore size, volume shrinkage and surface porosity values are represented in Table 1. The average pore size and porosity are maximum at $1650\,^{\circ}$ C. However, volume shrinkage changed incrementally as the sintering temperature increases.

4. Mathematical Modelling

Sintering experiments were conducted at different temperatures. The sintered samples were examined with SEM and images were analysed by using ImageJ software. Average pore diameters were measured for each pellets individually. After gathering the experimental data set, pore diameter and sintering temperature relation was investigated via a mathematical modelling. This model represents two distinct regions as shown in Figure 11 and it is compatible with experimental results in Figure 8.

This model was constructed by using piece-wise functions. They are derived from the experiment-analysis data set fit functions. Equations are written in Equations 3-4:

$$Pore(T) =$$

$$\begin{cases} -1.06 \times 10^{-7} \text{T}^3 + 0.00049 \text{T}^2 - 0.774 \text{T} + 398.62; \ 1425 \le \text{T} \le 1650 ^{\circ} \text{C} \ (3) \\ 95.91 \text{e}^{-0.003 \text{T}}; \qquad 1650 \le \text{T} \le 1800 ^{\circ} \text{C} \end{cases}$$
(4)

In the equation set, Pore(T) expresses the pore diameter in μm , and T defines the temperature in ${}^{\circ}C$. The mathematical relation is constructed on two pieces of function. However, it can be distinguished that sintering temperature and pore size are linearly dependent in the initial phase. There is a slight transition to second order polynomial relation from initial to intermediate phase. As appeared in Figure 12, it is modelled with two separate functions. Initial and intermediate stages are expressed with one function. The pore diameters are still getting higher dimensions with increased temperatures. At the

final phase, the pore diameter drastically decreases with increased sintering temperature. Therefore, this behaviour can be expressed with an exponential function which corresponds to 1650 - 1800 °C sintering temperature interval.

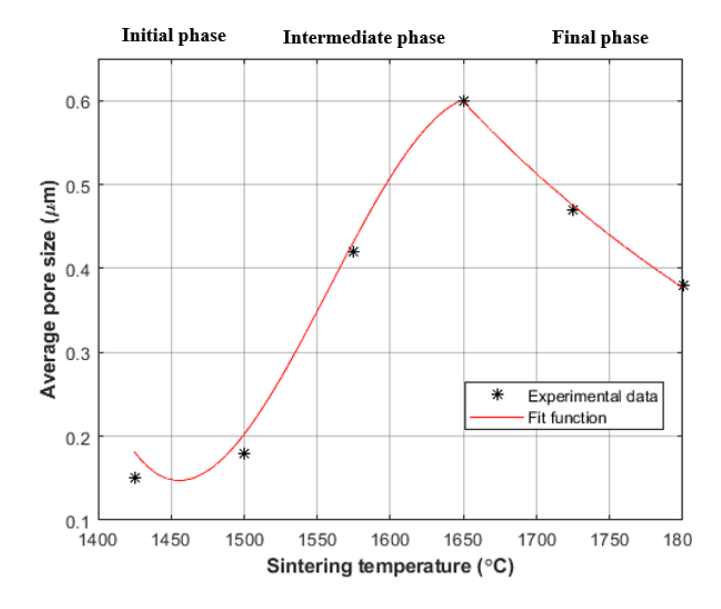


Figure 11. Sintering temperature and pore diameter relation

5. Conclusion

This study has demonstrated that sintering temperature plays a critical role in determining the microstructural and functional properties of r-CDT cathodes. The experimental results revealed that variations in sintering temperature directly influence the average pore size, surface porosity, and volume shrinkage of r-CDT pellets—all of which are key parameters affecting cathode emission performance, mechanical stability, and thermal behaviour. At lower sintering temperatures (1425–1500 °C), the structure retains high porosity with interconnected pores, favourable for emissive material transport but potentially limiting in terms of mechanical strength and thermal conductivity. As the sintering temperature increases (up to 1650 °C), pore size and porosity increase, reaching an optimum that balances material openness with improved structural coherence. Beyond 1650 °C, further increases in temperature lead to densification and a sharp reduction in both pore size and porosity due to pore closure and grain coalescence. This over-sintering effect may reduce emission efficiency by decreasing the available active surface area.

These findings confirm that the sintering temperature must be carefully controlled to tailor the r-CDT microstructure for desired operational conditions. The proposed mathematical model provides a valuable predictive tool for selecting the appropriate sintering parameters, allowing for efficient and

cost-effective optimization of cathode fabrication. Ultimately, controlling the sintering behaviour enables the design of scandate cathodes with superior emission stability, structural durability, and performance reliability in advanced vacuum electronic devices.

Overall, understanding the relationship between pore size and sintering temperature in dispenser cathodes is essential for tailoring their properties to meet specific performance requirements. By controlling sintering parameters, manufacturers can engineer cathodes with superior emission efficiency, thermal stability, and mechanical durability, ensuring reliable performance in demanding applications such as satellite communications, microwave tubes, and high-power electron devices.

Declaration of Competing Interest

The authors declare that they have no known competing financial interests or personal relationships that could have appeared to influence the work reported in this paper.

Funding

This study was funded by TÜBİTAK BİLGEM.

Acknowledgement

This study was supported by TÜBİTAK BİLGEM Cathode and Microwave Vacuum Tube Research Center.

Authors' Contributions

Zeynep Hazal Yazğan: Investigation, Methodology, Data curation, Writing – original draft, Writing – review & editing, Nergis Yıldız Angın Atmaca: Investigation, Methodology, Data curation, Writing – original draft, Writing – review & editing, Project administration, Okan Mert Yücedağ: Investigation, Methodology, Data curation, Writing – original draft, Writing – review & editing, Project administration

References

- [1] J. Xiu Bao, B. Fei Wan, *Appl. Surf. Sci.* (2006). https://doi.org/10.1016/j.apsusc.2005.08.012.
- [2] I.P. Melnikova, V.G. Vorozheikin, D.A. Usanov, *Appl. Surf. Sci.* (2003). https://doi.org/10.1016/S0169-4332(03)00289-7.
- [3] M.N. Seif, T.J. Balk, M.J. Beck, Appl. Surf. Sci. (2022). https://doi.org/10.1016/j.apsusc.2022.154541.
- [4] M.N. Seif, Q. Zhou, X. Liu, T.J. Balk, M.J. Beck, *IEEE Trans. Electron Devices*. (2022). https://doi.org/10.1109/TED.2022.3172052.
- [5] A. Shih, J.E. Yater, R. Abrams, Appl. Surf. Sci. (1999). https://doi.org/10.1016/S0169-4332(99)00062-8.
- [6] G.L. Davis, Powder Metall. (1979). https://doi.org/10.1179/pom.1979.22.3.145.
- [7] M. N. Seif, Q. Zhou, X. Liu, T. J. Balk ve M. J. Beck, (2022), https://doi.org/10.48550/arXiv.2202.04745
- [8] F. Andreola, C. Leonelli, M. Romagnoli, Am. Ceram. Soc. Bull, 79 (2000).
- [9] C. Selcuk, N. Morley, J. V. Wood, Powder Metall. (2005).

- https://doi.org/10.1179/003258905X37648.
- [10] S. Nakagawa, "Impregnated cathode and method for manufacturing the same" (United States Patent Application Publication, 2001), https://patents.google.com/patent/US20010019239A1/en. Accessed 20 May 2023
- [11] E.R. Kreidler, *J. Am. Ceram. Soc.* (1972). https://doi.org/10.1111/j.1151-2916.1972.tb13419.x.
- [12] M. Wang, K. Hu, R. Wu, K. Khanlari, F. Zhang, B. Lin, Adv. Powder Technol. (2023). https://doi.org/10.1016/j.apt.2023.104133.
- [13] Y. Cui, J. Wang, W. Liu, Y. Wang, M. Zhou, Appl. Surf. Sci. (2011). https://doi.org/10.1016/j.apsusc.2011.08.059.
- [14] N. Shinohara, M. Okumiya, T. Hotta, K. Nakahira, M. Naito, K. Uematsu, J. Am. Ceram. Soc. (2000). https://doi.org/10.1111/j.1151-2916.2000.tb01442.x.
- [15] R.M. German, Sintering Theory and Practice, (Wiley, New York, 1996), pp. 95-110.
- [16] Z. Hu, K. Lu, J. Am. Ceram. Soc. (2014). https://doi.org/10.1111/jace.13080.